MOLEKUL
eISSN: 2503-0310

Articles
https://doi.org/10.20884/1.jm.2024.19.1.9508

Silver-and-Sulphur-Codoped Fe_3O_4/TiO_2 as a Magnetically Separable Photocatalyst for Methylene Blue Degradation under Visible Light

Eko Sri Kunarti*, Dewi Agustiningsih, Fajar Inggit Pambudi, Stefen Rusli, and Bambang Rusdiarso

Department of Chemistry, Faculty of Mathematics and Natural Sciences, Universitas Gadjah Mada, Sekip Utara, Yogyakarta 55281, Indonesia

*Corresponding author email: eko_kunarti@ugm.ac.id

Received September 06, 2023; **Accepted** January 10, 2024; **Available online** March 20, 2024

ABSTRACT. This research aimed to investigate how the addition of silver and sulphur dopants modified the TiO_2 photocatalyst to enhance its responsiveness to visible light and improve its photocatalytic activity for methylene blue degradation. In addition, Fe_3O_4 was also added as a core to add magnetic properties to the photocatalyst material. The Fe_3O_4/TiO_2-Ag/S materials were prepared using $FeCl_3.6H_2O$ and $FeSO_4.7H_2O$ as the magnetite precursors, titanium tetraisopropoxide (TTIP) as the TiO_2 precursor, while $AgNO_3$ and CH_4N_2S were used as the sources for silver and sulphur dopants, respectively. The synthesized materials were next characterized using FT-IR, XRD, UV-Vis spectrophotometer, SEM-EDX, TEM, and VSM. The activity of the photocatalyst was then assessed through methylene blue degradation in a closed reactor involving various contained Ag:S ratios and reusability examination. The evaluation of photocatalytic degradation results was performed using UV-Vis spectrophotometry. Afterwards, the research findings indicate that the Fe_3O_4/TiO_2-Ag/S was successfully synthesized and exhibited magnetic properties with a saturation magnetization value of 5.33 emu/g. The highest photocatalytic activity (98.21%) was observed in Fe_3O_4/TiO_2-Ag/S (1:1) with a band gap energy value of 2.64 eV under visible light exposure at pH 10, 120 min, 10 mg mass of the photocatalyst, and methylene blue concentration of 5 mgL^{-1}. Furthermore, the Fe_3O_4/TiO_2-Ag/S photocatalyst was known to perform good stability through four reuse cycles.

Keywords: Dopants, Fe_3O_4/TiO_2-Ag/S, methylene blue, photocatalytic degradation

INTRODUCTION

Environmental pollution has emerged as a pressing concern, especially regarding dye waste pollution which needs urgent attention. The expanding global population has led to an increased demand for textiles, resulting in a heightened reliance on synthetic dyes. These dyes are favoured in the textile industry for their cost-effectiveness and durability, but improper waste management creates an environmental imbalance. Among these synthetic dyes is methylene blue, extensively employed as a colourant for textiles such as cotton, wool, and silk (Tebeje et al., 2022). Regrettably, the disposal of dye waste, including methylene blue, can give rise to severe health issues, such as dysfunctions in the kidneys, reproductive organs, liver, brain, and nervous system (Adegoke & Bello, 2015). Therefore, effective treatment of dye waste is crucial to mitigate these adverse impacts.

The photocatalytic method has shown promise in addressing dye waste treatment (Saggioro et al., 2016). This method involves generating radical species through oxidative reactions and promoting conductivity on the photocatalyst surface, thus accelerating the degradation of dyes. Additionally, the photocatalytic method offers advantages in terms of affordability and simplicity. Titanium dioxide (TiO_2) is a widely used photocatalyst material due to its non-toxic, readily available, and cost-effective nature. However, the efficacy of TiO_2 is limited to ultraviolet (UV) light exposure, which constitutes only about 5% of sunlight (Niu et al., 2013). Consequently, modifying TiO_2 to make it active under visible light exposure is necessary, and this can be achieved through the addition of dopants (Spadavecchia et al., 2014). Photocatalysts can be doped with single or dual dopants. Some studies have extensively investigated TiO_2 materials doped with single elements, including both metallic and non-metallic dopants, such as Ni-TiO_2, Ag-TiO_2, S-TiO_2, and N-TiO_2 (Chen et al., 2015; Devi & Kavitha, 2014; Leong et al., 2014; Pérez et al., 2015). However, single doping often results in a relatively high dopant-to-photocatalyst ratio. To address this limitation, the current study focuses on dual doping to investigate the impact of dopant ratios on reducing the band gap energy. Specifically, a mixture of metallic dopant (silver) and non-metallic dopant (sulphur) was utilized in this research. Silver exhibits surface plasmon resonance effects that enhance photon absorption from visible light, while the vacant *d* orbitals of sulphur act as efficient electron acceptors (Galbraith, 2007; Leong et al., 2014).

Another challenge related to TiO_2 lies in its challenging separation due to its propensity to disperse in water-based mediums. Given that the degradation of methylene blue occurs in a liquid medium, one of the solutions was found in coating TiO_2 onto a magnetic material such as Fe_3O_4. This coating imparts magnetic properties to the photocatalyst, enabling its convenient separation using an external magnet (Kunarti et al., 2018; Xie et al., 2019). The same approach was applied to TiO_2-Ag/S with varying concentrations of silver and sulphur in this study. This magnetic separation capability allowed for the reuse of the photocatalyst in the next cycle.

EXPERIMENTAL SECTION

Materials

The materials used in this study were chemicals with pro analysis quality including $FeCl_3.6H_2O$ (Merck), $FeSO_4.7H_2O$ (Merck), sodium citrate (Merck), $(NH_4)_2SO_4$ (Merck), $AgNO_3$ (Merck), absolute ethanol (Merck), titanium tetraisopropoxide (TTIP) 97% (Sigma-Aldrich), thiourea (Merck), NH_4OH 25% (Merck), methylene blue dye (Merck), N_2 gas (CV Putra Kembar), Milli-Q water (CV Progo Mulyo), and universal pH indicator (Merck).

Instrumentation

The instrumentations used in this research for material characterization comprise Fourier-Transform Infrared Spectrophotometer (Shimadzu Prestige 21), X-Ray Diffractometer (Shimadzu XRD 6000), Specular Reflectance UV-Visible spectrophotometer (Shimadzu 2450), UV-Visible spectrophotometer (GENESYS 10S), Transmission Electron Microscope (JEOL JEM-14000), Scanning Electron Microscope-Energy Dispersive X-Ray (Hitachi Flexsem 1000), and Vibrating Sample Magnetometer (OXFORD 1.2H).

Procedures

Synthesis of Fe_3O_4

The precursors including 5.4 g of $FeCl_3.6H_2O$ and 2.7 g of $FeSO_4.7H_2O$ were dissolved in 100 mL of Milli-Q water while being flushed with N_2 gas for 10 minutes. Subsequently, a 25% NH_4OH solution was added dropwise to the solution until a black Fe_3O_4 precipitate formed and sonicated for 1 h. The black Fe_3O_4 precipitate was then separated using an external magnet, washed, soaked in 50 mL of Milli-Q water overnight, and followed by the addition of 50 mL of 0.5 M sodium citrate solution. Lastly, the solution was left overnight and the final Fe_3O_4 solid was separated and dried at 100°C.

Synthesis of Fe_3O_4/TiO_2

A mixture of 0.1 g of $(NH_4)_2SO_4$ and 0.1 g of Fe_3O_4 powder was combined in 20 mL of ethanol and sonicated for 10 min. Next, 2.2 mL of titanium tetraisopropoxide (TTIP) and 2.5 mL of Milli-Q water were added to the mixture and sonicated for 3 h to form a precipitate. The obtained precipitate was then washed, separated, dried at 100 °C, and calcined at 500 °C for 3 h.

Synthesis of Fe_3O_4/TiO_2-Ag/S

The synthesized Fe_3O_4/TiO_2 was added with various masses of $AgNO_3$ and thiourea as the precursors of Ag and S dopants. The mass variation was made to produce Fe_3O_4/TiO_2-Ag/S with various ratios of Ag:S including 0:5, 1:2, 1:1, 2:1, and 5:0, the percentage of total dopants for each variation was 5% to the entire photocatalyst material. The whole mixture was next dispersed in Milli-Q water and sonicated for 3 h to form a precipitate. Afterwards, the precipitate was washed, separated, dried at 100 °C, and calcined at 500 °C for 3 h. The produced Fe_3O_4/TiO_2-Ag/S materials were finally characterized using FT-IR, XRD, SR-UV, and VSM spectrometer.

Catalytic activity and kinetic study

Methylene blue solution with a concentration of 5 mgL^{-1} and volume of 10 mL was prepared at pH 10, this solution was then added with Fe_3O_4/TiO_2-Ag/S photocatalyst stirred with a magnetic stirrer for various time intervals (0, 30, 60, 90, 120, and 150 min) under visible light exposure. Next, the absorbance of the methylene blue solution after photocatalytic degradation was measured using a UV-visible spectrophotometer at the wavelength of 665 nm. The same sequence of process was conducted on all photocatalyst materials with different ratios between Ag and S. For the reusability test, the Fe_3O_4/TiO_2-Ag/S photocatalyst was separated using an external magnet, dried, and reused for the subsequent degradation of methylene blue, following the same procedure. Lastly, the quantitative analysis of photocatalytic degradation was further studied by applying a pseudo-first-order kinetic model with the equation below (Rahmawati et al., 2023; Syoufian & Nakashima, 2008):

$$-(dC/dt) = k_{obs}C$$

in which,

$$k_{obs} = kK_{ads}[\bullet OH]$$

$$\ln C = -k_{obs}t + \ln C_0$$

where C is the concentration of methylene blue (mgL^{-1}), t is the reaction time (minutes), Kads is the adsorption constant of methylene blue on the TiO_2 surface (min^{-1}), and kobs is the observed rate constant for the photocatalytic degradation ($mgL^{-1}min^{-1}$). The term [•OH] is used to represent the total concentration of [•OH] produced during a photocatalytic reaction. Plots were made for the reaction time of 0 to 120 minutes as the optimum time observed.

RESULTS AND DISCUSSION

Figure 1 illustrates the infrared spectra of TiO_2, Fe_3O_4, Fe_3O_4/TiO_2, and Fe_3O_4/TiO_2-Ag/S with each Ag:S ratio, showcasing notable absorption peaks corresponding to the stretching vibration of the Ti-O bond at 553 cm^{-1} and the stretching vibration of O-H group at 3462 cm^{-1}. Additionally, a peak at 464 cm^{-1}

signifies the vibration of the Fe-O bond. The presence of citrate ions serving as magnetite-capping agents is indicated by some characteristic peaks. These include a distinct peak at 1635.64 cm^{-1} denoting the stretching vibration of the C=O group and some peaks observed at 2800-3000 cm^{-1} which indicate the stretching vibration of the Csp^3-H bond.

By analysing the FT-IR spectra further, it is evident that the intensity of Csp^3-H bond stretching vibration from citrate ions at 2800-3000 cm^{-1} diminished when the Ag:S ratio conducted was 1:1. This reduction in intensity was attributed to a larger TiO_2 surface area being modified by equal presence of Ag and S dopants. A peak at 1106 cm^{-1} confirms the presence of the stretching vibration from the S-O-Ti bond (Mutalib et al., 2022), this peak indicates that sulphur was successfully added to the TiO_2 framework as a dopant replacing some Ti core. Besides, the stretching vibration of Ag-O-Ti is also observed at 1385 cm^{-1} designating that Ag as a dopant was also well added to TiO_2 material (Rao et al., 2019). In addition, we can see here that the peaks representing the presence of two dopants do not show any significant intensities, this is because the amount of the dopant was very low compared to the photocatalyst material entirely.

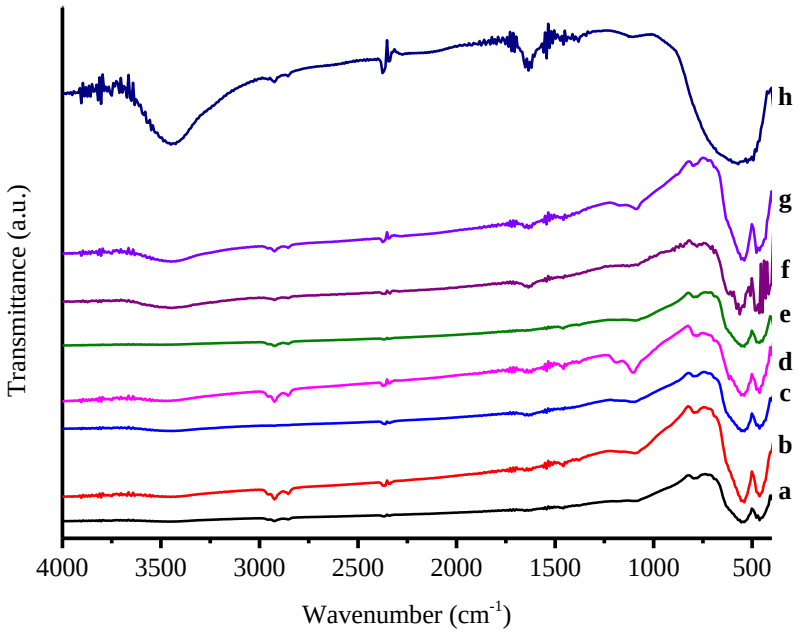

Figure 1. FT-IR spectra of Fe_3O_4/TiO_2-S (**a**), Fe_3O_4/TiO_2-Ag/S with Ag:S ratio of 1:2 (**b**), 1:1 (c), 2:1 (**d**), Fe_3O_4/TiO_2-Ag (**e**), Fe_3O_4/TiO_2 (**f**), Fe_3O_4 (**g**), and TiO_2 (**h**)

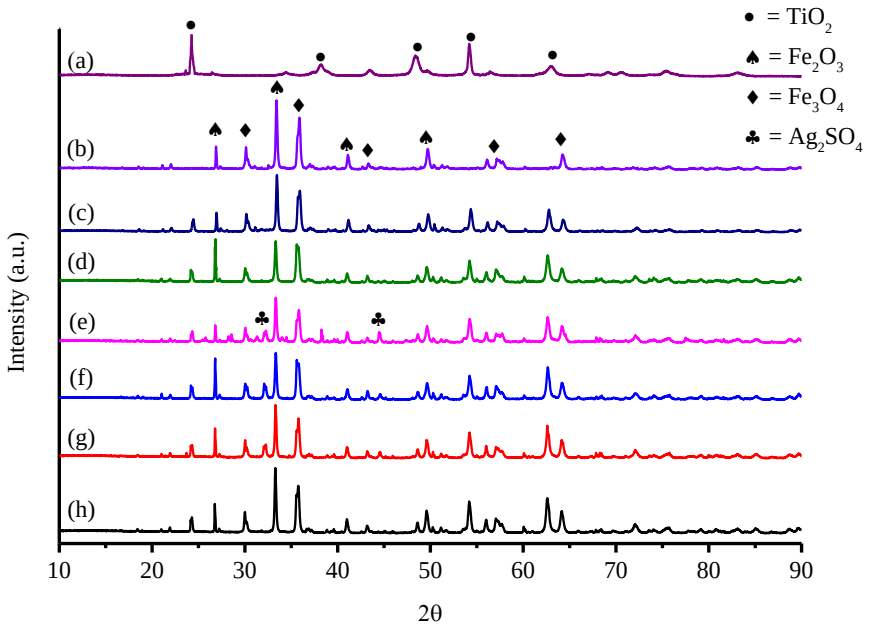

Figure 2. XRD pattern of TiO_2 (**a**), Fe_3O_4 (**b**), Fe_3O_4/TiO_2 (**c**), Fe_3O_4/TiO_2-S (**d**), Fe_3O_4/TiO_2-Ag/S with Ag:S ratio of 1:2 (**e**), 1:1 (**f**), 2:1 (**g**), and Fe_3O_4/TiO_2-Ag (**h**)

Figure 2 displays the diffraction pattern of Fe_3O_4/TiO_2-Ag/S with all Ag:S ratios, revealing the characteristic peaks corresponding to TiO_2 anatase at 2θ of 24.5°, 38°, 48°, 54°, and 63° along with its respective hkl values of (101), (112), (200), (105), and (213). These findings align with the ICDD (International Centre for Diffraction Data) of TiO_2 anatase (PDF Number 021-1272). In addition, the peaks at 2θ 31°, 35°, 43°, 57 °, and 63° indicate the presence of Fe_3O_4 with hkl values of (220), (311), (400), (511), and (440), respectively. This pattern is in accordance with the magnetite database obtained from ICDD (PDF Number 007-0322). However, as we can see from the diffractogram above hematite (Fe_2O_3) was also observed as contained magnetic material beside magnetite. It is presented by some peaks at 26°, 33°, 41°, and 49°, along with its hkl values of (012), (104), (113), and (024), respectively based on hematite ICDD (PDF Number 013-0534). This phenomenon might have occurred due to the probable phase transformation from Fe_3O_4 to Fe_2O_3 after it contacted atmospheric O_2 and encountered an oxidation process.

Even if each material consists of a different percentage ratio of Ag:S, there is no peak observed representing the distinguishable properties between each photocatalyst. This is because the total amount of Ag and S (5%) was way too low compared to the whole photocatalyst components, therefore the dopants did not contribute any significant peaks. Moreover, as can be seen from **Figure 2**, there are some peaks at 2θ of 32° and 45° corresponding to hkl values of (110) and (202) from Ag_2SO_4 based on ICDD (PDF Number 029-1442). The formation of Ag_2SO_4 originated from some sulphur species which reacted with Ag^+ ions.

A method used to identify the modifications in TiO_2 involved analysing the material's absorption toward UV and visible light using a UV-visible spectrophotometer (SR-UV). The reflectance spectra of all synthesized materials are depicted in **Figure 3** (**a**). We also did further analysis for SR UV-Vis data using the Kubelka-Munk equation to find the exact band gap energy value of each material, the plots built from this analysis are displayed in **Figure 3** (**b**). The data obtained from this calculation are then listed in Table 1. According to the table, the incorporation of silver and sulphur dopants led to a reduction in the band gap energy. This effect can be attributed to the silver dopant, in the form of Ag^+ and Ag species, and sulphur dopant, as S^{4+} and S^{6+} species, which occupied energy levels just below the conduction band. These dopants acted as electron acceptors due to their empty *d* orbitals which readily accepted the excited electrons. Furthermore, the presence of plasmon resonance in the silver dopant caused the captured electrons to oscillate, effectively lowering the band gap energy value. Consequently, the Fermi level below the conduction band in Fe_3O_4/TiO_2-Ag/S led to the band gap energy decrease compared to TiO_2 and Fe_3O_4/TiO_2.

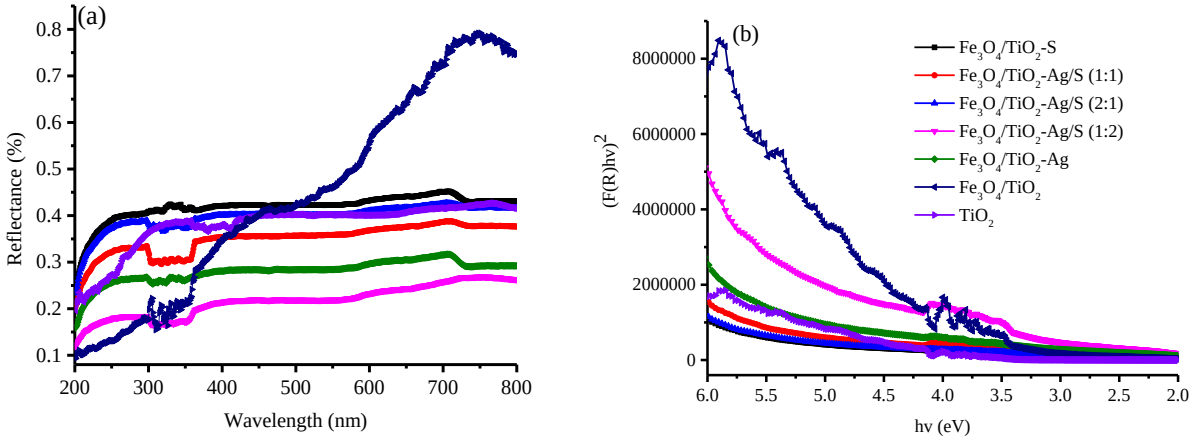

Figure 3. SR UV-Vis spectra (**a**) and Kubelka-Munk derivation plot (**b**) of the synthesized materials

Table 1. Band gap energy of synthesized photocatalysts

Photocatalyst	Band gap energy (eV)
Fe_3O_4/TiO_2-Ag	2.83
Fe_3O_4/TiO_2-Ag/S (2:1)	2.81
Fe_3O_4/TiO_2-Ag/S (1:1)	2.64
Fe_3O_4/TiO_2-Ag/S (1:2)	2.69
Fe_3O_4/TiO_2-S	2.81
Fe_3O_4/TiO_2	3.13
TiO_2	3.33

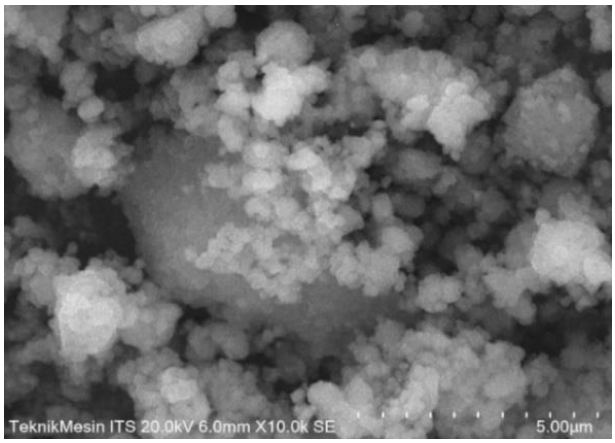

Figure 4. BSE-SEM image of Fe_3O_4/TiO_2-Ag/S (1:1)

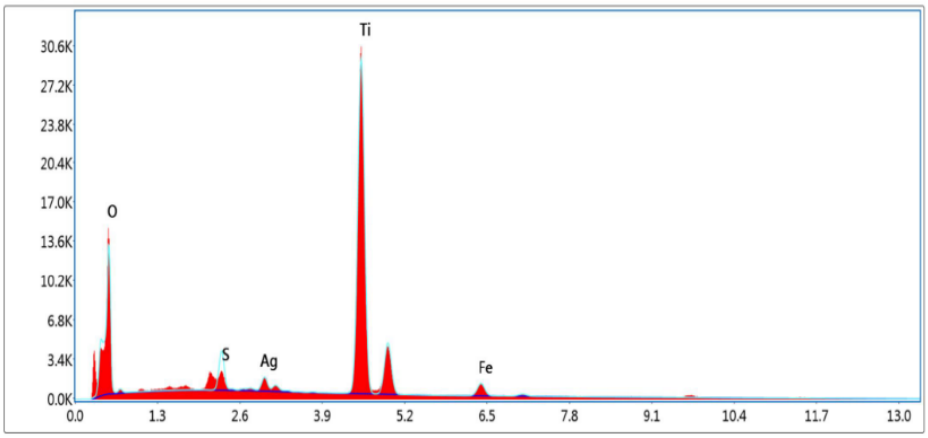

Figure 5. EDX spectra of Fe_3O_4/TiO_2-Ag/S (1:1)

Table 2. Percentage of constituent elements in Fe_3O_4/TiO_2-Ag/S (1:1)

Element	Weight percentage (%)	Atomic percentage (%)
Ag	2.17	0.50
Fe	3.30	1.47
O	46.67	72.52
S	2.57	2.00
Ti	45.29	23.51

Furthermore, among all photocatalysts, Fe_3O_4/TiO_2-Ag/S (1:1) was observed to have the lowest band gap energy value of 2.64 eV. This value is lower than the outcome reported by Kunnamareddy et al. (2018), who found a band gap energy of 2.89 eV for TiO_2-Ag/S (1:1). Conversely, Fe_3O_4/TiO_2-Ag/S materials with other Ag:S percentage ratio exhibited an increase in band gap energy. This phenomenon could be caused by two factors. Firstly, the Burstein-Moss effect might have occurred due to the relative abundance of one dopant (either sulphur or silver) which accepted electrons and led to a heightened electron density near the conduction band. Thereby, this resulted in an elevated Fermi level and an increase in the band gap energy. Secondly, there was likely a specific quantity of undoped sulphur species with a negative charge that interacts with Ag^+ ions, forming Ag_2SO_4 species.

SEM-EDX analysis was carried out in this study to investigate the morphology and distribution of Ag and S dopants on Fe_3O_4/TiO_2 surfaces. The outcome of BSE-SEM characterization for Fe_3O_4/TiO_2-Ag/S (1:1) material is illustrated in Figure 4. According to that result, it is known that the synthesized Fe_3O_4/TiO_2-Ag/S material demonstrates a spherical shape with even distribution. The presence of Ag atoms is indicated by the lighter part in the image, attributed to their higher electron density compared to Fe, Ti, O, and S atoms. Besides, the EDX data shown in **Figure 5** and Table 2 demonstrate that all constituent elements in Fe_3O_4/TiO_2-Ag/S (1:1) comprising Ag, Fe, O, S, and Ti atoms were successfully detected with their relative percentages. In this research, TEM characterization was conducted to examine the morphology and particle size of the synthesized material. Both Fe_3O_4/TiO_2-Ag/S (1:1) and TiO_2-Ag/S

(1:1) materials display a spherical shape, as observed in **Figures 7** (**a**) and (**b**), respectively. According to the TEM images, it is noticed that photocatalyst particles were formed in nano-dimension, with the particle sizes generally under 50 nm. The formation of these nanoparticles was attributed to the presence of sodium citrate solution as the capping agent during the synthesis process.

As shown in **Figure 7**, it is noticed that Fe_3O_4/TiO_2-Ag/S (1:1) material was easily separated by using an external magnet. Consequently, the Fe_3O_4/TiO_2-Ag/S photocatalyst exhibited the recoverable aspect, enabling easy retrieval within a separation time of three minutes. To quantitatively assess the magnetic properties, a Vibrating Sample Magnetometer (VSM) analysis was performed. This investigation aimed to examine changes in magnetic characteristics, which can be observed through the reduction in saturation magnetization (Ms) values. As indicated in Figure 8, the highest saturation magnetization (Ms) was achieved in the magnetic hysteresis curve spectrum of Fe_3O_4 material, amounting to 27.45 emu/g. Conversely, the saturation magnetization (Ms) for Fe_3O_4/TiO_2 and Fe_3O_4/TiO_2-Ag/S materials are lower than Fe_3O_4 with values of 8.50 emu/g and 5.33 emu/g, respectively. This reduction in saturation magnetization was attributed to at least two factors. Firstly, the dipolar interaction between the magnetic core in Fe_3O_4 weakened due to the coverage of the Fe_3O_4 surface by TiO_2. Secondly, there was likely a change in magnetic polarization with electron delocalization from Fe^{2+} in magnetite towards the TiO_2 surface. Consequently, the spin polarization decreased and led to a decline in Ms values. Additionally, the presence of silver dopants may also contribute to the decrease in spin polarization, as electrons from Fe^{2+} and TiO_2 can be delocalized to Ag nanoparticles, resulting in the lowest saturation magnetization value.

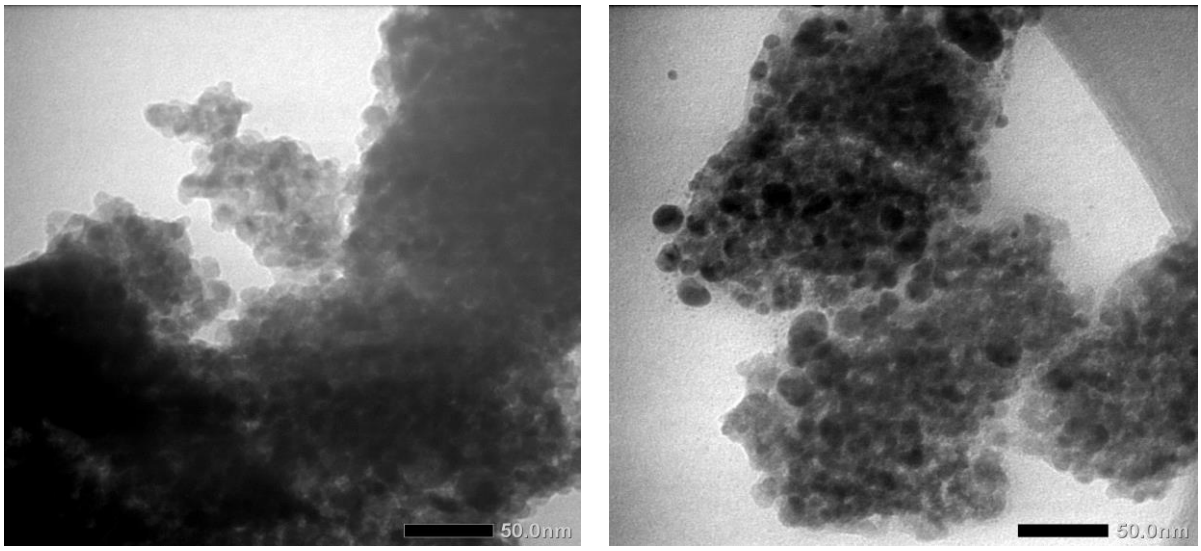

(**a**) (**b**)

Figure 6. TEM image of Fe_3O_4/TiO_2-Ag/S (1:1) (**a**) and TiO_2-Ag/S (1:1) (**b**)

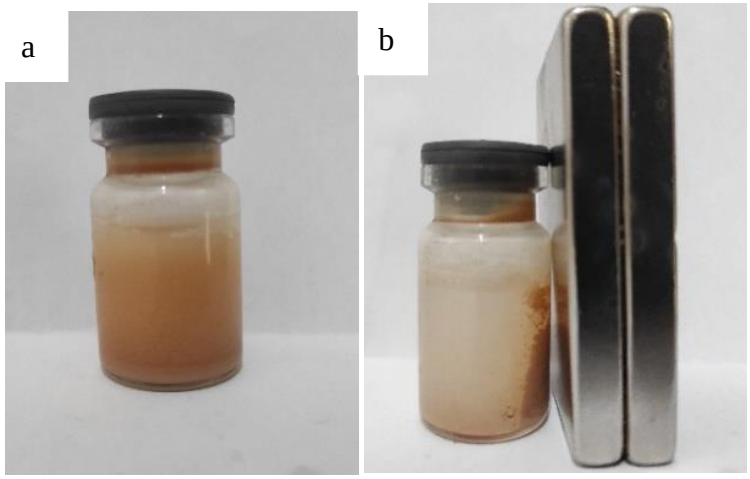

Figure 7. The visual image of Fe_3O_4/TiO_2-Ag/S (1:1) before (**a**) and after (**b**) being separated by an external magnet

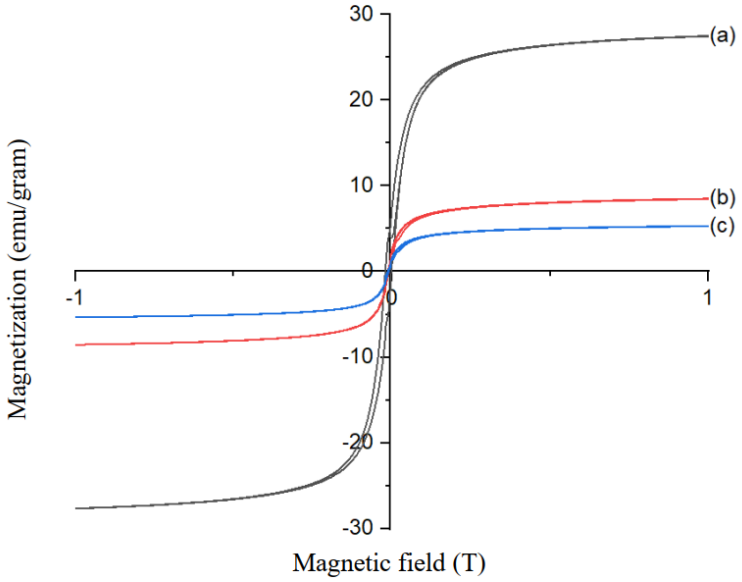

Figure 8. Magnetic-hysteresis curve of Fe_3O_4 (**a**), Fe_3O_4/TiO_2 (**b**), Fe_3O_4/TiO_2-Ag/S (1:1) (**c**)

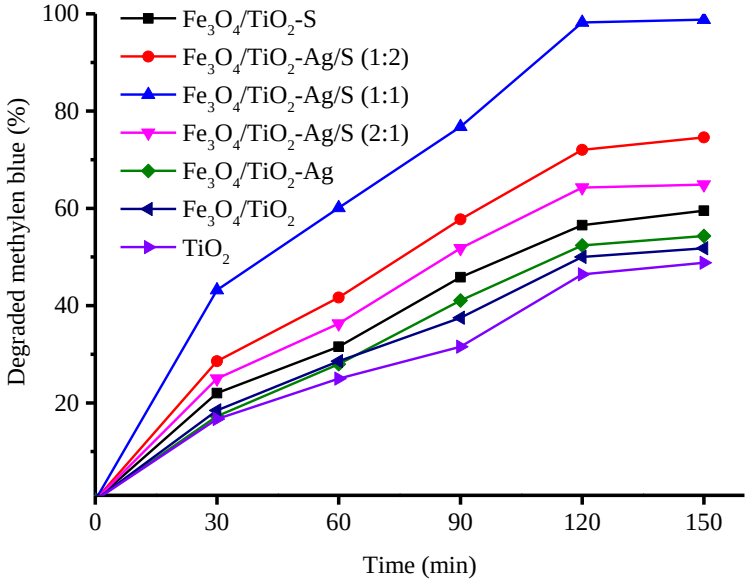

Figure 9. Performance of each photocatalyst in methylene blue degradation over time

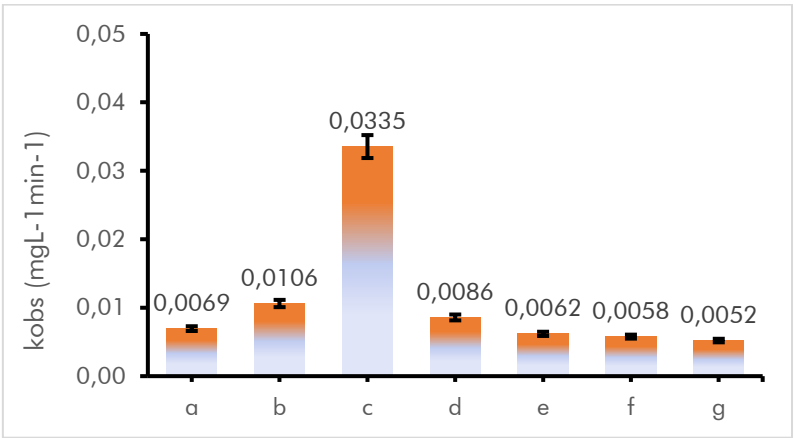

Figure 10. The observed rate constant of Fe_3O_4/TiO_2-S (**a**), Fe_3O_4/TiO_2-Ag/S (1:2) (**b**), Fe_3O_4/TiO_2-Ag/S (1:1) (**c**), Fe_3O_4/TiO_2-Ag/S (2:1) (**d**), Fe_3O_4/TiO_2-Ag (**e**), Fe_3O_4/TiO_2 (f), and TiO_2 (**g**) in methylene blue degradation at 120 min

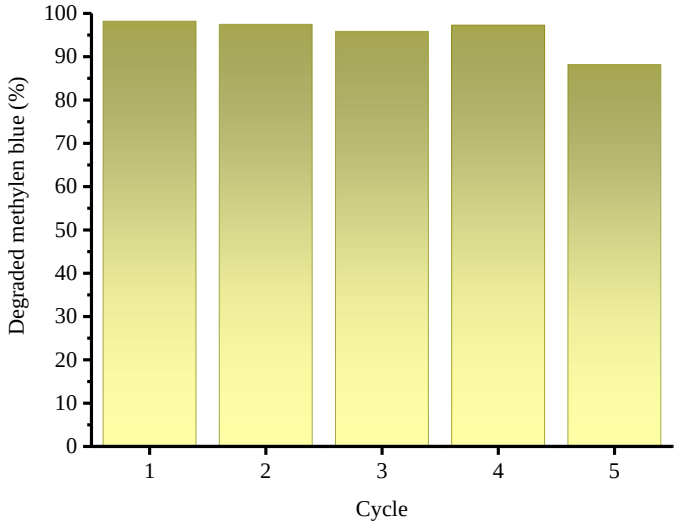

Figure 11. Reusability test of Fe_3O_4/TiO_2-Ag/S (1:1) at optimum condition

In this research, we also elucidated the procedure for evaluating the efficiency of the synthesized photocatalyst materials in degrading methylene blue compounds. The evaluation commenced by identifying the maximum absorption wavelength of methylene blue through the utilization of a UV-visible spectrophotometer, revealing it to be 665 nm. The decision to set the reaction pH value of the methylene blue solution at 10 was based on the previous research done by Nasikhudin et al. (2018), demonstrating that the most effective photocatalytic degradation using TiO_2 was reached at this pH level. This is because the interaction between the negatively charged TiO^- species and the cationic methylene blue molecules played a critical role in facilitating photocatalytic degradation.

Moreover, the duration of light exposure also influenced the degradation process, where longer exposure time resulted in a higher degradation rate of methylene blue due to the increased formation of OH• (hydroxyl) and $O_2^{\bullet -}$ (superoxide) radicals. The optimum reaction time was obtained to be 120 minutes, as extended irradiation led to a constant degradation rate. As shown in **Figure 9**, the ratio of Ag:Ti in the photocatalyst material significantly impacted the degradation efficiency, with a 1:1 ratio of Ag:Ti yielding the best result (98.21%). Besides that, the low band gap energy of Fe_3O_4/TiO_2-Ag/S (1:1) successfully enhanced light absorption and yielded improved photocatalytic performance. Conversely, other photocatalysts with different Ag:S ratios exhibited lower degradation rates due to their larger band gap energies. This impeded electron conduction and reduced the number of holes in the valence band responsible for generating OH• (hydroxyl) and $O_2^{\bullet -}$ (superoxide) radicals. Doping-induced modifications in photocatalyst materials resulted in significantly increased activity when compared to pure TiO_2 and Fe_3O_4/TiO_2 composite. This phenomenon underscores the crucial role played by Ag and S dopants in enhancing the overall photocatalytic activity of these materials. Furthermore, Fe_3O_4/TiO_2 exhibited improved performance compared to pure TiO_2 when exposed to visible light, which is in line with its lower band gap energy value. Besides, the adsorption factor also had a considerable influence as Fe_3O_4 can act as an adsorbent, although the impact of photocatalytic degradation remained dominant.

Additionally, this research also explored the photocatalytic degradation kinetics of methylene blue, involving various Ag:S percentage ratios. The kinetic study presented in Figure 10 suggests that the Fe_3O_4/TiO_2-Ag/S (1:1) material performed the highest rate constant for photocatalytic degradation, measured at $3.354.10^{-2}$ $mgL^{-1}min^{-1}$.

The reusability test result shown in **Figure 11** demonstrates that the overall yield of the methylene blue photocatalytic degradation was remarkably high, indicating that the Fe_3O_4/TiO_2-Ag/S (1:1) material was sufficiently stable for multiple uses. However, there was a slight decline in degradation efficiency after the fifth cycle, it was possibly due to the methylene blue solution covering the surface of the photocatalytic material which obstructed the visible light penetration towards the photocatalyst surface. Similar behaviour was also observed by Kunnamareddy et al. (2018) in their study of methylene blue degradation using TiO2-Ag/S (1:1) photocatalyst.

CONCLUSIONS

The Fe_3O_4/TiO_2-Ag/S material has been successfully synthesized confirmed by some characterization results from FT-IR, XRD, UV-Vis spectrophotometer, SEM-EDX, TEM, and VSM. It displayed both good magnetic properties and excellent responsiveness to visible light, with the lowest band gap energy (Eg) value of 2.64 eV for Fe_3O_4/TiO_2-Ag/S (1:1). Notably, this photocatalyst material achieved the optimum performance for methylene blue degradation with degraded percentage of 98.21% and rate constant of $3.354.10^{-2}$ $mgL^{-1}min^{-1}$. The Fe_3O_4/TiO_2-Ag/S

photocatalyst also exhibited exceptional chemical stability, allowing for five reuse cycles while maintaining high photocatalytic activity. In the future, certain modifications may be necessary to enhance the efficacy of the photocatalyst. This would enable it to possess greater potential as a separable photocatalyst for the degradation of various forms of chemical waste.

REFERENCES

Adegoke, K. A., & Bello, O. S. (2015). Dye sequestration using agricultural wastes as adsorbents. *Water Resources and Industry*, *12*, 8–24. https://doi.org/10.1016/j.wri.2015.09.002

Chen, J., Qiu, F., Xu, W., Cao, S., & Zhu, H. (2015). Recent progress in enhancing photocatalytic efficiency of TiO_2-based materials. *Applied Catalysis A: General*, *495*, 131–140. https://doi.org/10.1016/j.apcata.2015.02.013

Devi, L. G., & Kavitha, R. (2014). Enhanced photocatalytic activity of sulfur doped TiO_2 for the decomposition of phenol: A new insight into the bulk and surface modification. *Materials Chemistry and Physics*, *143*(3), 1300–1308. https://doi.org/10.1016/j.matchemphys.2013.11.038

Galbraith, J. M. (2007). On the role of d orbital hybridization in the chemistry curriculum. *Journal of Chemical Education*, *84*(5), 783–787. https://doi.org/10.1021/ed084p783

Kunarti, E.S., Kartini, I., Syoufian, A., & Widyandari, K.M. 2018. Synthesis and photoactivity of Fe_3O_4/TiO_2-Co as a magnetically separable visible light responsive photocatalyst. *Indonesian Journal of Chemistry,* 18(3), 403-410.

Kunnamareddy, M., Diravidamani, B., Rajendran, R., Singaram, B., & Varadharajan, K. (2018). Synthesis of silver and sulphur codoped TiO_2 nanoparticles for photocatalytic degradation of methylene blue. *Journal of Materials Science: Materials in Electronics*, *29*(21), 18111–18119. https://doi.org/10.1007/s10854-018-9922-2

Leong, K. H., Gan, B. L., Ibrahim, S., & Saravanan, P. (2014). Synthesis of surface plasmon resonance (SPR) triggered Ag/TiO_2 photocatalyst for degradation of endocrine disturbing compounds. *Applied Surface Science*, *319*(1), 128–135. https://doi.org/10.1016/j.apsusc. 2014.06.153

Mutalib, M. A., Ludin, N. A., Su'ait, M. S., Davies, M., Sepeai, S., Teridi, M. A. M., Noh, M. F. M., & Ibrahim, M. A. (2022). Performance-enhancing sulfur-doped TiO_2 photoanodes for perovskite solar cells. *Applied Sciences*, *12*(1). https://doi.org/10.3390/app12010429

Nasikhudin, Diantoro, M., Kusumaatmaja, A., & Triyana, K. (2018). Study on photocatalytic properties of TiO_2 nanoparticle in various pH condition. *Journal of Physics: Conference Series*, *1011*(1). https://doi.org/10.1088/ 1742-6596/1011/1/012069

Niu, Y., Xing, M., Zhang, J., & Tian, B. (2013). Visible light activated sulfur and iron co-doped TiO_2 photocatalyst for the photocatalytic degradation of phenol. *Catalysis Today*, *201*(1), 159–166. https://doi.org/10.1016/j.cattod.2012.04.035

Pérez, E., Torres, M. F., Morales, G., Murgia, V., & Sham, E. (2015). Synthesis of N-TiO_2 effect of the concentration of nitrogen in the band gap. *Procedia Materials Science*, *8*, 649–655. https://doi.org/10.1016/j.mspro.2015.04.121

Rahmawati, L., Kurniawan, R., Prasetyo, N., Sudiono, S., & Syoufian, A. (2023). Copper-and-nitrogen-codoped zirconium titanate (Cu-N-$ZrTiO_4$) as a photocatalyst for photo-degradation of methylene blue under visible-light irradiation. *Indonesian Journal of Chemistry*, *23*(2), 416–424. https://doi.org/10.22146/ijc.78908

Rao, T. N., Riyazuddin, Babji, P., Ahmad, N., Khan, R. A., Hassan, I., Shahzad, S. A., & Husain, F. M. (2019). Green synthesis and structural classification of *Acacia nilotica* mediated-silver doped titanium oxide (Ag/TiO_2) spherical nanoparticles: Assessment of its antimicrobial and anticancer activity. *Saudi Journal of Biological Sciences*, *26*(7), 1385–1391. https://doi.org/10.1016/j.sjbs.2019.09.005

Saggioro, E. M., Oliveira, A. S., & Moreira, J. C. (2016). Heterogeneous photocatalysis remediation of wastewater polluted by indigoid dyes. *Textile Wastewater Treatment*. https://doi.org/10.5772/63790

Spadavecchia, F., Ceotto, M., Presti, L. Lo, Aieta, C., Biraghi, I., Meroni, D., Ardizzone, S., & Cappelletti, G. (2014). Second generation nitrogen doped titania nanoparticles: A comprehensive electronic and microstructural picture. *Chinese Journal of Chemistry*, *32*(12), 1195–1213. https://doi.org/10.1002/cjoc.201400502

Syoufian, A., & Nakashima, K. (2008). Degradation of methylene blue in aqueous dispersion of hollow titania photocatalyst: Study of reaction enhancement by various electron scavengers. *Journal of Colloid and Interface Science*, *317*(2), 507–512. https://doi.org/10.1016/ j.jcis.2007.09.092

Tebeje, A., Worku, Z., Nkambule, T. T. I., & Fito, J. (2022). Adsorption of chemical oxygen demand from textile industrial wastewater through locally prepared bentonite adsorbent. *International Journal of Environmental Science and Technology*, *19*(3), 1893–1906. https://doi.org/10.1007/s13762-021-03230-4

Xie, E., Zheng, L., Li, X., Wang, Y., Dou, J., Ding, A., & Zhang, D. (2019). One-step synthesis of magnetic-TiO_2-nanocomposites with high iron oxide-composing ratio for photocatalysis of rhodamine 6G. *PLoS ONE*, *14*(8), 1–19. https://doi.org/10.1371/journal.pone.0221221